7-2009

Observed 1970-2005 cooling of summer daytime temperatures in coastal California

Bereket Lebassi

Jorge González González

Drazen Fabris
Santa Clara University, dfabris@scu.edu

Edwin P. Maurer
Santa Clara University, emaurer@scu.edu

Norman L. Miller

See next page for additional authors

Recommended Citation

Lebassi, B., J. Gonzalez, D. Fabris, E. Maurer, N. Miller, C. Milesi, P. Switzer, and R. Bornstein, 2009, Observed 1970-2005 cooling of summer daytime temperatures in coastal California, J. Climate Vo. 22, 3558-3573, doi:10.1175/2008JCLI2111.1

Authors
Bereket Lebassi, Jorge González González, Drazen Fabris, Edwin P. Maurer, Norman L. Miller, Cristina Milesi, Paul Switzer, and Robert Bornstein

Observed 1970–2005 Cooling of Summer Daytime Temperatures in Coastal California

BEREKET LEBASSI,* JORGE GONZÁLEZ,* DRAZEN FABRIS,* EDWIN MAURER,+ NORMAN MILLER,#
CRISTINA MILESI,@ PAUL SWITZER,& AND ROBERT BORNSTEIN**

* *Department of Mechanical Engineering, Santa Clara University, Santa Clara, California*
+ *Department of Civil Engineering, Santa Clara University, Santa Clara, California*
# *Climate Science Department, Lawrence Berkeley National Laboratory, Berkeley, California*
@ *University Corporation at Monterey Bay, Seaside, and NASA Ames Research Center, Mountain View, California*
& *Department of Statistics, and Department of Environmental and Earth Systems Science, Stanford University, Stanford, California*
** *Department of Meteorology, San José State University, San José, California*

(Manuscript received 22 June 2007, in final form 18 November 2008)

ABSTRACT

This study evaluated 1950–2005 summer [June–August (JJA)] mean monthly air temperatures for two California air basins: the South Coast Air Basin (SoCAB) and the San Francisco Bay Area (SFBA). The study focuses on the more rapid post-1970 warming period, and its daily minima temperature T_{min} and maxima temperature T_{max} values were used to produce average monthly values and spatial distributions of trends for each air basin. Additional analyses included concurrent SSTs, 40-yr European Centre for Medium-Range Weather Forecasts (ECMWF) Re-Analysis (ERA-40) sea level coastal pressure gradients, and GCM-downscaled average temperature T_{ave} values.

Results for all 253 California National Weather Service (NWS) Cooperative Observer Program (COOP) sites together showed increased T_{ave} values (0.23°C decade^{-1}); asymmetric warming, as T_{min} values increase faster than T_{max} values (0.27° versus 0.04°C decade^{-1}) and thus decreased daily temperature range (DTR) values (0.15°C decade^{-1}). The spatial distribution of observed SoCAB and SFBA T_{max} values exhibited a complex pattern, with cooling (−0.30°C decade^{-1}) in low-elevation coastal areas open to marine air penetration and warming (0.32°C decade^{-1}) in inland areas. Results also showed that decreased DTR values in the basins arose from small increases at inland sites (0.16°C decade^{-1}) combined with large decreases (−0.58°C decade^{-1}) at coastal sites. It is also possible that some of the current observed temperature trends could be associated with low-frequency decadal variability, expected even with a constant radiative forcing.

Previous studies suggest that cooling JJA T_{max} values in coastal California were a result of increased irrigation, coastal upwelling, or cloud cover. The current hypothesis is that they arise (as a possible ''reverse reaction'') from the global warming of inland areas, which results in increased sea-breeze flow activity. GCM model T_{ave} warming decreased from 0.13°C decade^{-1} at inland sites to 0.08°C decade^{-1} in coastal areas. Sea level pressure increased in the Pacific high and decreased in the thermal low. The corresponding gradient thus showed a trend of 0.04 hPa 100 km^{-1} decade^{-1}, supportive of the hypothesis of increased sea-breeze activity.

1. Introduction

Long-term daily 2-m air temperature trends generally show diurnal asymmetric warming rates, as nighttime minima temperatures T_{min} have warmed faster than daytime maxima values T_{max}, which thus decreases daily temperature range (DTR). Karl et al. (1993) attributed this effect to increased evaporation from increased sea surface temperatures (SSTs), which increased relative humidity and cloud cover and thus decreased incoming solar radiation and T_{max}. The radiative–convective model of Stenchikov and Robock (1995) showed that solar reflection and absorption by aerosols also reduced T_{max} warming rates. Modeling of stable nocturnal boundary layers by Walters et al. (2007) showed that increased greenhouse gases (GHGs) reduce nocturnal IR cooling and thus increase T_{min} values.

Asymmetric warming has also been attributed to anthropogenic land cover conversions on global (Mintz 1984; Zhang et al. 1996) and regional (Chase et al. 2000) scales (e.g., deforestation increases T_{min}; Lawton et al.

Corresponding author address: Jorge González, NOAA/CREST Professor, City College of New York, Steinman Hall (T-238), New York, NY 10031.
E-mail: gonzalez@me.ccny.cuny.edu

DOI: 10.1175/2008JCLI2111.1

2001; Defries et al. 2002; Nair et al. 2003). Urban heat islands (UHIs; Bornstein 1968; Landsberg 1981; Gallo et al. 1993; Pon et al. 2000) also increase T_{min}, whereas irrigation decreases T_{max} (Betts 2001), as it converts arid regions to (slower warming) moist high-thermal-inertia vegetated plains (Pielke et al. 2002, 2007). Regional climate modeling by Kueppers et al. (2007) showed that western U.S. irrigation lowers average T_{ave} and T_{max} values at rates comparable to increases from GHG warming. Modeling by Lobell et al. (2006) showed that temperature changes were generally dominated by GHG warming, but large fractional land-use changes can locally dominate.

Modeling by Snyder et al. (2003) showed that increased GHGs also enhance coastal upwelling by increasing land–ocean pressure and temperature gradients, as land areas warm faster than ocean areas because of thermal differences. The increased gradients also enhance alongshore winds that produce upwelling, which further increases onshore temperature gradients. McGregor et al. (2007) observed this effect over coastal northwest Africa, whereas Bakun (1990) had hypothesized a similar scenario to explain an observed 30-yr increase of upwelling along the coast of California. Alfaro et al. (2006) found average March–May Pacific decadal oscillation (PDO) values and June–August (JJA) SSTs correlated with JJA T_{ave} values with maximum correlations in coastal regions. LaDochy et al. (2007) found similar results but also showed that T_{max} and PDO values were uncorrelated.

Analysis of 80 yr of annually averaged T_{ave} daily values at 112 National Weather Service (NWS) Cooperative Observer Program (COOP) sites in California by Goodridge (1991) showed warming in coastal (attributed to warming SSTs) and inland urban (attributed to UHI effects) areas (an observed cooling in inland rural areas was unexplained). Nemani et al. (2001) found summertime asymmetric warming at northern California COOP sites in the Napa and Sonoma Valleys during 1951–97, as T_{min} values increased and T_{max} values slightly decreased; both effects were attributed to a measured increase in cloud cover. Increased annual dewpoint temperatures (T_D) over coastal California were related to increased SST values.

Interpolated (to a grid) California COOP monthly averaged T_{ave} values from 1950–99 by Duffy et al. (2007) showed warming in all seasons, attributed to increased UHIs or GHGs. Christy et al. (2006) analyzed 1910–2003 data from 18 Central Valley (CenV) COOP sites and showed increased T_{ave} and T_{min} values in all seasons, with greater summer and fall increases. They also found concurrent summer cooling T_{max} and warming T_D values, with changes attributed to increased summer irrigation. Bonfils and Duffy (2007) argued, however, that the warming T_{min} values were not due to irrigation, which they said could only overcome GHG-warming effects on T_{max}. Bonfils and Lobell (2007) and Lobell and Bonfils (2008) showed that expanded irrigation cooled these summer T_{max} values but produced negligible effects on T_{min} values.

Analysis by LaDochy et al. (2007) of data from 331 California COOP sites during 1950–2000 also showed annual T_{ave} values warming at most stations. Almost all increases were due to changes in T_{min}, as T_{max} showed either no change or cooling; the fastest T_{min} increases occurred in summer. Although maximum T_{ave} warming occurred in Southern California areas, its northeast interior basin showed cooling, also found by Christy et al. (2006). Abatzoglou et al. (2009) also found significant negative trends in late summer and early fall T_{max} values along the immediate California coast over the previous three decades. California coastal cooling of annual T_{ave} values is seen as a single data point in the global 2001 Intergovernmental Panel on Climate Change (IPCC) observational dataset (Jin 2004).

Although previous studies have generally attributed observed decreased summer maximum temperatures during the last decades at COOP sites in coastal California to increased UHIs, cloud cover, upwelling, and/or irrigation, the current study uses the same data to determine the spatial distributions of these decreases in two important California air basins and then to relate them to sea breeze–induced marine air penetration patterns. In addition, the study provides evidence that onshore sea breezes have increased during the study period.

2. Methodology

The study focuses on two highly populated near-sea level coastal California regions: the South Coast Air Basin (SoCAB) and San Francisco Bay Area (SFBA), which includes the northern CenV. Data were obtained from the National Climatic Data Center (NCDC) for 273 California COOP sites (Fig. 1), and they consisted of 1953–2005 JJA 2-m daily T_{min} and T_{max} air temperatures, as hourly values are not available from COOP sites. J. T. Abatzoglou (2008, personal communication) developed an objective means to detect climate inhomogeneities in monthly-mean T_{min}, T_{max}, and T_{ave} values at COOP stations across California. They found that although individual station inhomogeneities can influence its trends, no widespread or geographically coherent inhomogeneities were identified across the state for the period of 1970 to the present. COOP data from stations in California have thus been used in many of the studies discussed in

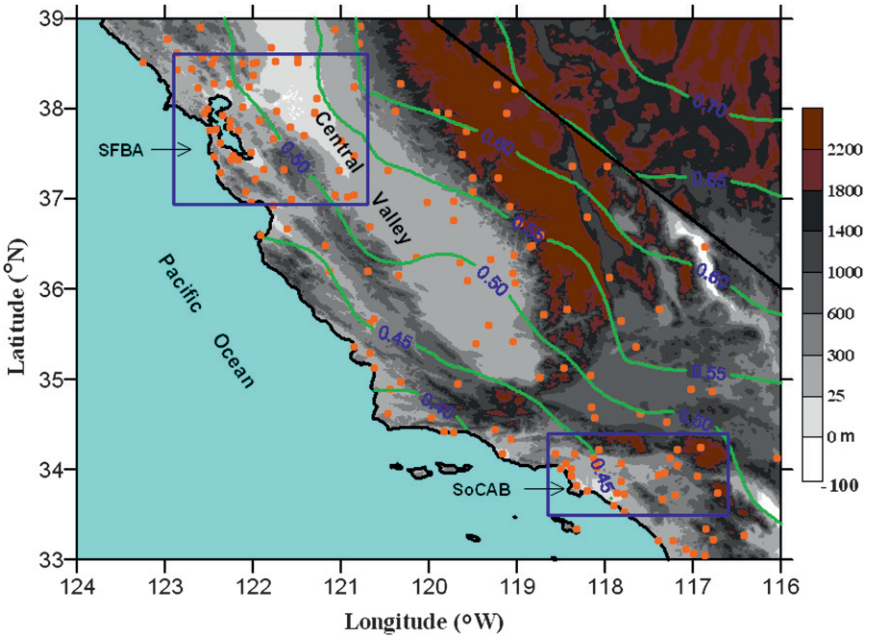

FIG. 1. Central California topographic heights (m), COOP sites (orange dots), California–Nevada border (sloping straight line), air basins of Figs. 3, 4 (blue boxes), and linearly interpolated (on 0.5° grid resolution) 2-m 1950–99 GCM summer average temperature change (°C).

section 1. The subperiod of 1970–2005 is the main focus of the study, as it shows the most rapid global warming.

The following criteria eliminated incomplete datasets: months with >5 days of missing data, years with <2 months of data, and sites with >15 yr of missing data. These criteria eliminated 23 of the 273 sites, leaving 52 in the SFBA and 28 in the SoCAB. The number of sites retained in a given year averaged 240 and ranged between 217 and 250, whereas 226 sites had >30 yr of data, 23 had between 20 and 29 yr, and only one had <20 yr. Resulting daily T_{min} and T_{max} values at each site were used to produce average JJA T_{min}, T_{max}, T_{ave}, and DTR values for California for each year.

A linear trend was fit to each of these annual time series using simple least squares linear regression on time, separately for the two periods of interest: 1953–69 and 1970–2005. Standard calculations of statistical significance (p values) of the fitted trend against the hypothesis of chance deviations from a flat trend were done. The standard method is to compute a t statistic and then to report a two-sided p value as the chance probability of observing a t value numerically larger than the calculated t statistic. The p values give the probabilities that the trend of the observed magnitude over the observation period occurred by chance, and hence a low p value means that the results are significant.

Formulas for the t statistic may be found in any elementary textbook, such as Mann (2007). When the two-tail test was applied to the 81 SoCAB and SFBA sites, 33 had $p \leq 0.01$ (i.e., very significant), 7 were in the range of >0.01 to ≤ 0.05 (i.e., significant), 6 were in the range of >0.05 to ≤ 0.10 (i.e., somewhat significant), and 35 were in the range of >0.10 (i.e., not significant), where the terminology is arbitrary. Note that the inclusion of instrument error (if it could be evaluated) would lower these significant levels; this correction is not made in most similar studies.

The question of whether statistically significant year-to-year autocorrelation in trend residuals or deviations (i.e., differences between observations and fitted trends) exist was also considered. Autocorrelation implies a better-than-chance predictability of residuals, based on the preceding residuals for a given time series. In the presence of statistically significant autocorrelation, one would need to reduce the effective number of observations, which in turn would decrease the value of the t statistic. To achieve statistical significance at $p = 0.05$, the empirical autocorrelation of resid uals from the fitted trend would need to be $>1.65/N^{1/2}$ [i.e., approximately 0.27 for a time series with a sample size (N) of 36 annual values]. Statistically significant residual autocorrelation for the time series on the current time series was found for only 12 of the 81 SoCAB and SFBA sites, and thus no adjustments were made to N for any of the 81 sites.

The 1970–2005 T_{max} trend at each site in the SoCAB and SFBA air basins was plotted at their corresponding

station locations, together with an indication of the statistical significance of each trend value (see Figs. 3, 4). As strong topographic distortions of surface flow patterns in both basins have been observed (Hayes et al. 1984; CARB 1989; MacKay 1997), this information was used to subjectively construct spatial distribution patterns of observed trend values in each air basin. Subjective analysis was necessary, as interpolation software cannot fully account for topographic distortions of most meteorological fields (though some can approximate topographic influences on wind flow patterns). Spatial temperature-trend plots are useful for qualitative pattern interpretation, and no station trend value was ''violated'' in their construction. For the SoCAB, 23 of the sites had >30 yr of data, 4 had 20–29 yr, and only 1 had <20 yr; the corresponding SFBA numbers were 49, 2, and 1.

The resulting spatial patterns of coastal cooling (i.e., negative trend value) and inland warming (i.e., positive trend value) in each air basin are discussed below. The positive trend subregions are herein referred to as inland warming regions and the negative trend subregions as coastal cooling regions; why such an interpretive division based on calculated trends could be meaningful is discussed below.

As was done for the four all-California parameters, a combined linear trend for the 1970–2005 T_{max} values were calculated separately for the combined (i.e., SoCAB plus SFBA) coastal cooling subareas and then for the combined inland warming subareas. The mean value for each station over the period was determined, and then the time series of deviations from the station mean for each year of the record was determined. Linear trends were then calculated by combining all of the coastal cooling station deviations in both air basins and then likewise for all of their inland warming stations. Statistical p values were not calculated for these subarea trends, because the analysis is ''exploratory'' (i.e., exact subarea boundaries in each basin were based on observed station trends, rather than on an a priori division based on physical principles). Note that these boundaries do generally agree with the known basin flow patterns discussed above, even though the exact inland extent of the cooling areas could not be determined a priori.

Mean monthly JJA SSTs along California at a 2.5° grid resolution were obtained from NCDC. These extended reconstructed SST (ERSST) values, from the International Comprehensive Ocean–Atmosphere Data Set (ICOADS), had been produced by statistical methods that allow for stable reconstructions from sparse data (Smith and Reynolds 2003). A single 1950–2005 average SST trend was thus calculated for the ocean area in Fig. 1.

Coastal-to-inland pressure trends from 1979 (i.e., the year satellite data were first assimilated) to 2002 were calculated using JJA monthly-mean 40-yr European Centre for Medium-Range Weather Forecasts (ECMWF) Re-Analysis (ERA-40) high-resolution (T85, 1.4° resolution) reanalysis sea level pressures. The plotted value at each grid point represents its linear trend during the period. A slight mismatch exists between the periods of the temperature and pressure analyses (i.e., 1970–2005 versus 1979–2002, respectively), but this should not significantly effect results. Values are available (available online at http://dss.ucar.edu/datasets/ds126.0/) at 6-h intervals, starting at 0500 LT (where LT = UTC minus 7 h during summer DST periods); 1100 LT values were used as an estimate of sea-breeze initiation. Pressure gradient trends were calculated separately for the SFBA and SoCAB coastal areas using differences between values at the closest offshore and closest onshore grid ECMWF grid points in each basin. An analysis (not shown) indicates that the pressure gradient trends showed a variation, actually changing signs, during the diurnal period, supporting the current use of the 0500 LT data. The lack of appropriate pressure observational sites precludes any meaningful analysis of such pressure gradient trends from NWS observational data.

Averaged 1950–99 T_{ave} values from 11 general circulation models (GCMs) with 2° grid resolutions over California were obtained from the IPCC Fourth Assessment World Climate Research Programme (WCRP) Coupled Model Intercomparison Project phase 3 (CMIP3) archive. Values were linearly interpolated to a 0.5° resolution grid; additional details can be found in Maurer (2007).

3. Results

a. Local flow patterns

California summer climate is dominated by atmospheric and oceanic features, which include the Pacific high, coastal ocean current system, and continental thermal low (with an axis from the Mexican plateau to central California). The Pacific high creates alongshore wind stresses on the ocean surface, which results in spring and summer upwelling of cold water to the surface (Hickey 1979; Bakun 1990; Herbert and Schuffert 2001; McGregor et al. 2007). Climate variability can produce small changes in these features and thus large variations in coastal climate (Gilliland 1980); for example, during El Niño years, upwelling diminishes and SSTs increase along the coast of California (Simpson 1983).

These features also produce strong pressure, temperature, and moisture gradients as well as a nearly

continuous summer daytime onshore, cool, moist Pacific Coast monsoon marine airflow (Williams and DeMandel 1966; Giorgis 1983; Miller and Schlegel 2006). Subsidence from the Pacific high also produces an elevated inversion layer (up to 20°C through a 250-m layer) that caps the shallow (<1 km deep) marine boundary layer (MBL). The inversion base is lowest just off the coast, where upwelling water results in MBL cooling (Seaman et al. 1995).

Knowledge of local topographic effects on marine air intrusions is essential to understanding study-area flow patterns. The CenV of California is about 800 km long and 80 km wide (Fig. 1), with the Sacramento Valley (SacV) as its northern third and the San Joaquin Valley (SJV) its southern two-thirds. It is bordered by a continuous mountain barrier of at least 1500 m in elevation: Klamath on its northwest, Cascades on its northeast, and Sierra Nevada on its east. Its western border is the coastal range (elevation of 915 m), with the following low-elevation inlets from the ocean into the SacV (Fig. 2a): 1) Golden Gate Gap (GGG), a sea level passage into San Francisco Bay; 2) Estero Lowlands, near sea level and north of San Francisco; and 3) San Bruno Gap, south of San Francisco (elevation of 61 m).

Channeling through the GGG produces a westerly jet, which fans into three branches: southward into the Santa Clara Valley; northward into the Petaluma, Sonoma, and Napa Valleys of Marin; and eastward to the Carquinez Strait (Root 1960). The air in the strait passes the Sacramento River Delta and goes halfway into the CenV (at its central latitude), where it splits northward into the SacV and southward into the SJV (Blumenthal et al. 1985). This onshore-directed marine flow is augmented by thermally driven daytime upslope flows along the east-facing slopes of the coastal and inland mountain ranges (Seaman et al. 1995). As nighttime land surfaces cool more rapidly than the sea, a thus reversed temperature gradient produces evening offshore-directed land-breeze flows, also augmented by similarly directed downslope mountain flows along the west-facing slopes.

Analogous SoCAB flow patterns are dominated by the same general circulation features. The area, however, is a coastal plain open to the ocean, with mountain ranges (peaks to 3000 m) on three sides (Fig. 2b). Resulting daytime onshore-directed marine air intrusions into the SoCAB are thus more widespread than those into the CenV, and the inland movement of its MBL (with an overwater depth of about 150 m) resembles a cold front (McElroy and Smith 1991). The onshore marine flow splits northward into the San Fernando Valley and eastward to Chino, where it splits into northward (toward the San Gabriel and San Bernardino Mountains) and southeastward (toward the Lakeview and Estelle Mountains) directed flows. Marine air can be prevented from exiting the basin (between the San Gabriel and San Bernardino Mountains) by opposing upper-level easterly flows associated with mesoscale high pressure areas north of that gap (Boucouvala et al. 2003).

b. Spatial patterns

This section presents the spatial distributions of the SoCAB and SFBA T_{max} warming and cooling trends found in the current study. A comparison with previous literature results is presented in section 4, as is a proposed explanation of the current and literature results.

The spatial distribution of observed SoCAB 1970–2005 JJA T_{max} values (Fig. 3) exhibits a complex pattern, with cooling in low-elevation coastal areas open to marine air penetration and warming at both inland and higher-elevation coastal areas. Marine air enters at the low-elevation coastal area south of Palos Verdes (Fig. 2b) and then splits northward toward the San Fernando Valley (with a maximum cooling of -0.99°C decade^{-1}) and eastward toward the Chino Hills, where it splits again. One part flows northward, toward the foothills between the San Gabriel and San Bernardino Mountains, whereas its southern branch flows past the Lakeview and Estelle Mountains. Although these regions thus show cooling, higher-elevation inland regions (which lack marine air penetration) show warming: north of Lakeview (local maximum of 0.12°C decade^{-1}), over the San Gabriel and San Bernardino Mountains to the north (local maximum of 0.41°C decade^{-1}), and south of the Santa Ana Mountains (local maximum of 0.64°C decade^{-1}).

Given a data scarcity in some areas, some trend-line segments were placed based on an understanding of topographic influences on near-surface flow patterns (e.g., southern end of the -0.2°C decade^{-1} trend line in the Estelle Valley was justified by the increasing elevation in that area). The 0.0°C decade^{-1} trend-line section between the San Gabriel and San Bernardino Mountains was likewise placed, whereas the 0.4°C decade^{-1} dashed trend line near the San Gabriel Mountains was added for continuity with that over the San Bernardino Mountain. Sites north of the San Fernando Valley would allow for a more precise northern edge of that cooling area.

As SFBA topography is more complex, so are its concurrent 1970–2005 JJA T_{max} spatial warming and cooling patterns (Fig. 4). As its coastal ranges almost completely block marine air penetration, flow through the GGG (Fig. 2a) into the SFBA splits northward

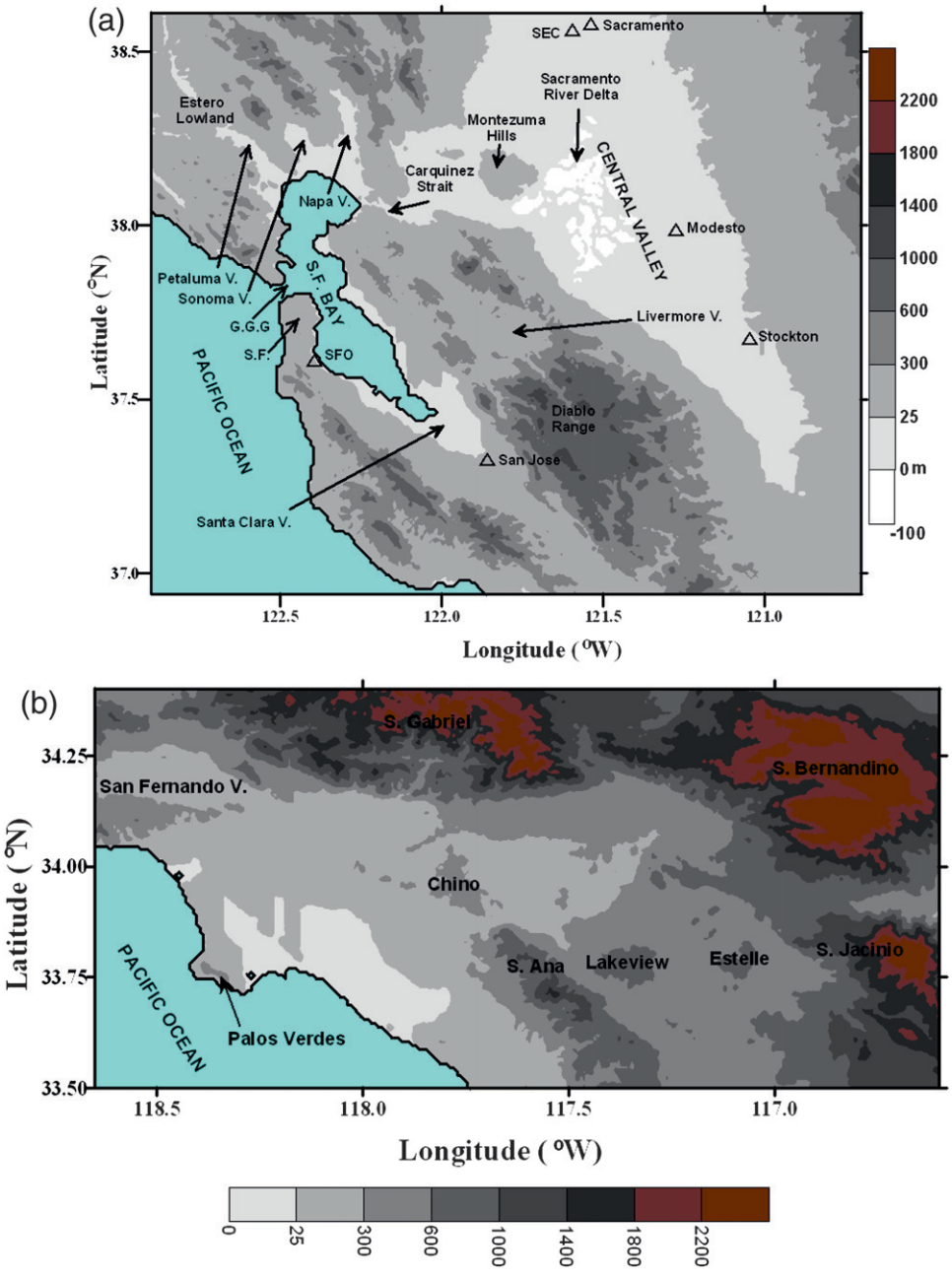

FIG. 2. Topographic heights (m) and geographic locations mentioned in text for (a) SFBA and (b) SoCAB study areas.

toward the Petaluma, Sonoma, and Napa Valleys and meets southward flowing marine air from the Estero Lowlands; these valleys are thus cooling (local max of -0.69°C decade^{-1}). Some GGG air also flows southward along San Francisco Bay into the Santa Clara Valley; cooling sites thus exist on both sides of the bay (local max of -0.53°C decade^{-1}). Some of the flow through the GGG also splits off southward into the Livermore Valley, where all sites are cooling (local max of -0.60°C decade^{-1}). The remainder of this air enters the SacV through the Carquinez Strait, where it splits at the Montezuma Hills into northward and southward flows (local max cooling of -0.33°C decade^{-1}). The most rapidly cooling area, however, is over Monterey Bay (local max of -0.73°C decade^{-1}). As the onshore flow from the bay and the southward flow from the Santa Clara Valley frequently are prevented from converging by the southern extension of the Santa Cruz

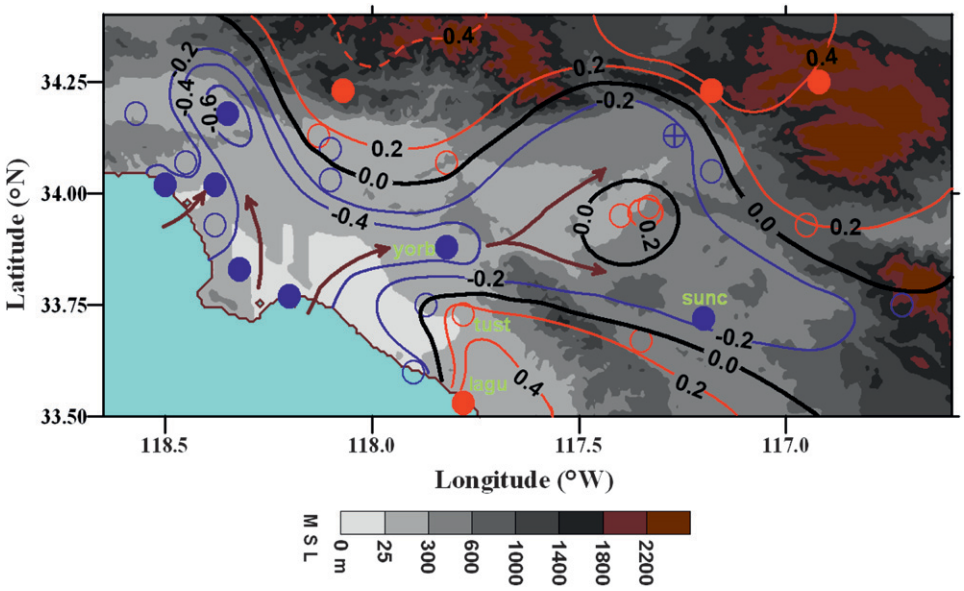

FIG. 3. Spatial distribution of SoCAB 2-m summer maximum-temperature trends (°C decade^{-1}) for 1970–2005; arrows indicate predominant summer daytime flow-patterns; blue, red, and black colors indicate cooling, warming, and no-change isopleths and station locations; dashed isopleths are extrapolated; and statistical p values of $\geq$0.01, between 0.01 and $\leq$0.05, between 0.05 and $\leq$0.1, and $>$0.1 are represented, respectively, by full-colored, half-colored, plus signs, and open circles. The four indicated site names (in green) are discussed in the text.

Mountains, two separate −0.2°C decade^{-1} isotherms are shown.

Warming regions, however, exist along the eastern side of the SacV and in higher-elevation areas on its perimeter. The eastern-edge warming (local max of 0.29°C decade^{-1}) is probably associated with wake effects from the high-elevation outcrop south of the Montezuma Hills. Warming is also seen in the hills east of San Francisco Bay (local max of 0.72°C decade^{-1}) and in the coastal hills (local max of 0.50°C decade^{-1}) between the San Francisco and Monterey Bay cooling areas.

Given SFBA topographic complexity and data scarcity, part of one trend line was again placed based on the physical reasoning discussed above (e.g., the end of −0.2°C decade^{-1} isotherm south of the San Francisco Bay could have been linked with that northeast of its current southern edge). Additional observational sites would be useful to better define the edges of several cooling/warming areas (e.g., some within the mountain area south of the Livermore Valley would allow for more precise location of the northern edge of the 0.2°C decade^{-1} trend line in the southeast part of the domain, whereas additional sites in the SacV delta would have allowed for more precise location for its 0.0°C decade^{-1} trend line). Observational sites west of the Petaluma Valley and in the hills west of the delta would have likewise been useful to show the western edges of their cooling areas.

A scatterplot was constructed to show T_{max} cooling and warming trends versus inland distance from the coast, with low- and high-elevation sites shown with different symbols. This was done only for the generally ''open to the sea'' SoCAB domain and not for the SFBA domain because of its complex topography (i.e., three chains of hills parallel to coast). Results (not shown) generally showed: 1) cooling at low-elevation (i.e., below the optimum value of 200 m) coastal stations and 2) warming at higher-elevation coastal and most inland stations (regardless of elevation). Four unexplained outliers were seen (Fig. 3): for example, warming at low-elevation Tustin Ranch in Irvine (Tust) at 36-m MSL and Laguna Beach (Lagu) at 11-m MSL and cooling at higher-elevation Yorba Linda (Yorb) at 357 m and Sun City (Sunc) at 43 m. Additional data analyses and/or mesomet modeling are needed to understand these outliers.

c. *Temporal-trend slopes*

Mean JJA 2-m T_{ave} trends for all 253 California COOP sites used in the present study show the expected warming (Fig. 5a) during both the 1950–70 and 1970–2005 periods with increases of 0.10° and 0.15°C decade^{-1}, respectively. The later-period trend is, as expected from

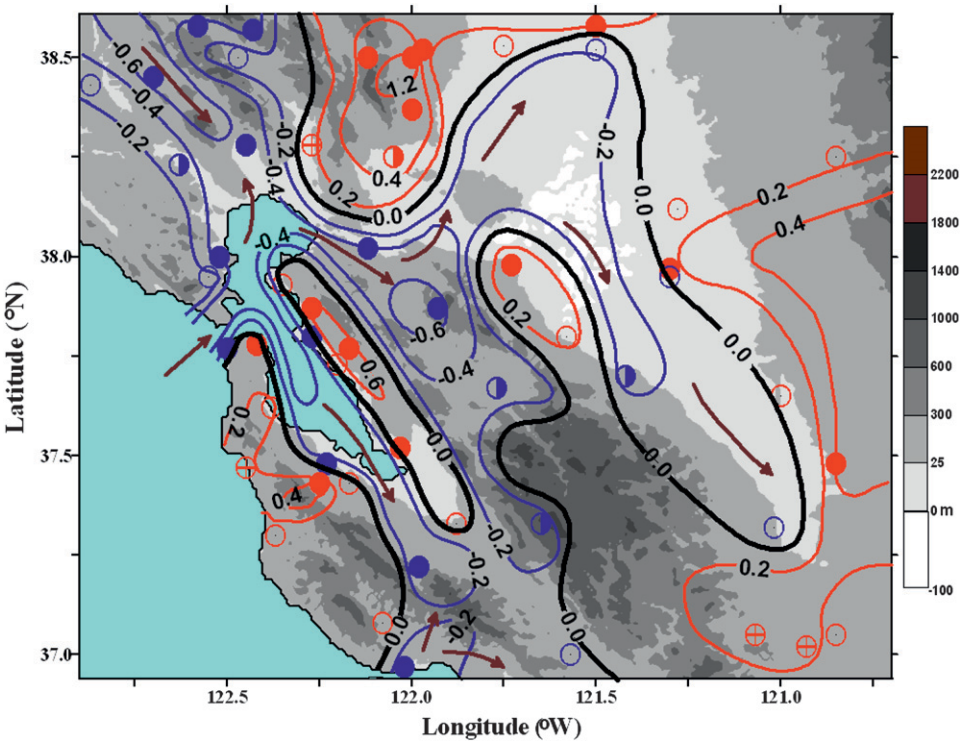

FIG. 4. Same as Fig. 3 but for SFBA.

the literature discussed in section 1, larger than the earlier-period trend, as is true for the other three parameters in Figs. 5b–d. Only latter-period p values for each parameter are thus given in Table 1; the p value for JJA California T_{ave} values is 0.03, representing only a 3% probability of observing a trend of this magnitude by chance. Corresponding T_{min} values also show an expected larger latter-period warming (Fig. 5b) (i.e., 0.16° and 0.27°C decade^{-1}, respectively) with an even smaller (than for T_{ave}) latter-period p value of 0.01 in Table 1.

Corresponding T_{max} values show the expected asymmetric warming (i.e., T_{max} trends $<$ T_{min} trends) during both periods (Fig. 5c versus Fig. 5b), with increases of 0.05° and 0.04°C decade^{-1}, respectively. These all-California T_{max} trends are small and nonsignificant (Table 1), as the large inland warming and coastal cooling trends of Figs. 3, 4 have combined to yield a small, insignificant net trend. Concurrent DTR values (Fig. 5d) have thus decreased during both periods (−0.10° and −0.23°C decade^{-1}, respectively) as expected; the latter-period p value for trend is 0.06, borderline statistically significant.

As a comparison to the all-California trends in Fig. 5, combined JJA trends for 1970–2005 were computed separately for the interpreted coastal cooling and inland warming subareas of Figs. 3, 4 for each of the above four temperature parameters. As the resulting combined inland warming-area (Fig. 6a; Table 1) T_{max} increase was unexpectedly (all such unexpected results are discussed in next section) greater than its T_{min} increase (0.32° versus 0.12°C decade^{-1}), its T_{ave} value increased at an intermediate rate (0.24°C decade^{-1}) and its DTR values increased by 0.16°C decade^{-1}.

The corresponding coastal cooling area T_{min} value unexpectedly increased (Fig. 6b; Table 1) at a greater rate than the corresponding inland warming (Fig. 6a) value (0.28° versus 0.16°C decade^{-1}), whereas the absolute magnitude of its T_{max} cooling rate was about the same as that for the inland warming area (−0.30° versus 0.32°C decade^{-1}). Its T_{ave} value thus changed by only −0.01°C decade^{-1} and its DTR decreased by −0.58°C decade^{-1}. Statistical p values were not calculated for any subarea trend estimates because these analyses are exploratory, as discussed above.

4. Discussion

This section compares the current results with those in the literature (as described in section 1) and then offers a hypothesis and supporting data to explain them. Previous studies (e.g., Duffy et al. 2007; LaDochy et al.

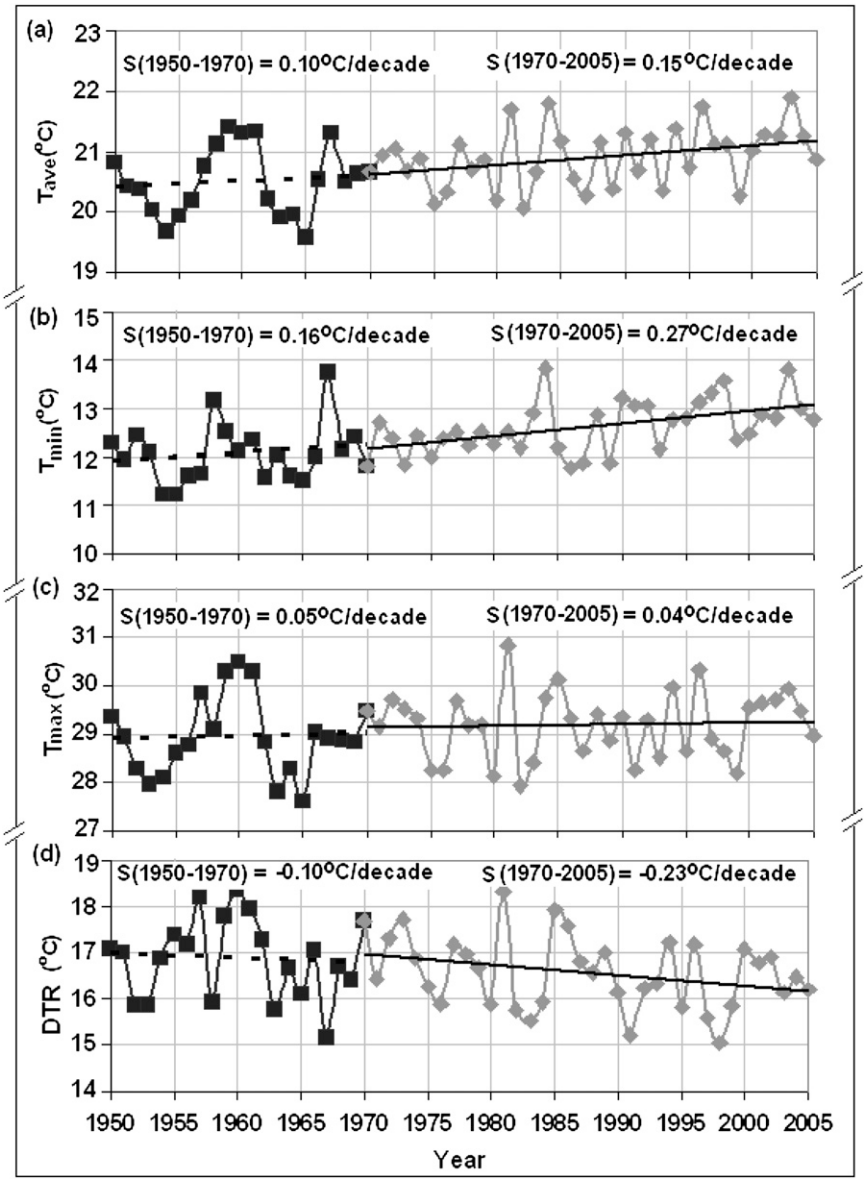

FIG. 5. Summer 1950–1970 and 1970–2005 California 2-m temperate trends (summer; °C decade^{-1}): (a) average, (b) minimum, (c) maximum, and (d) range (DTR) values.

2007) have also used 1950–2005 summer (JJA) COOP data and have found some or all of the following current all-California results: 1) increased T_{ave} values; 2) asymmetric warming, as T_{min} values increase faster than T_{max} values; and 3) thus, decreased DTR values.

The current results also show coastal valley sites with JJA increased T_{min} and decreased T_{max} values. Previous studies that likewise found these results include Nemani et al. (2001) for the SFBA, Christy et al. (2006) and Bonfils and Lobell (2007) for the CenV, and LaDochy et al. (2007) for the SoCAB. Although these studies also generally also found concurrent decreased DTR values for these valleys, LaDochy et al. (2007) found increased values at 30 of 219 sites. Although the current study likewise showed decreased JJA DTR values for all California sites taken together, it found that this arose from combined DTR increases at inland warming sites and larger DTR decreases at coastal cooling sites. Previous observational studies have suggested that the summer cooling of T_{max} values in California were due to increased irrigation (e.g., Christy et al. 2006; Bonfils and Lobell 2007), coastal upwelling (e.g., Bakun 1990; Goodridge 1991), or cloud cover (e.g., Nemani et al. 2001). Modeling studies have also attributed this cooling

TABLE 1. Observed 1970–2005 summer (JJA) average T_{ave}, T_{min}, T_{max}, and DTR warming or cooling trends for all California COOP sites, as well as for combined SoCAB plus SFBA coastal cooling and inland warming subareas.

	Trend (°C decade^{-1})		
		SoCAB–SFBA subareas	
Parameter	All California	Inland warming	Coastal cooling
T_{ave}	0.15[a]	0.24	−0.01
T_{min}	0.27[b]	0.16	0.28
T_{max}	0.04[c]	0.32	−0.30
DTR	−0.23[d]	0.16	−0.58

[a] Statistical p value ≥0.05.
[b] Statistical p value ≥0.01.
[c] Statistical p value >0.1.
[d] Statistical p value ≥0.1.

to either increased upwelling (e.g., Snyder et al. 2003) or irrigation (e.g., Kueppers et al. 2007).

The current hypothesis is that observed coastal California JJA cooling of T_{max} values arises from GHG-induced global warming of inland areas, which results in increased sea-breeze flow activity, which in turn overwhelms (as discussed below) GHG warming of coastal areas. This hypothesis is consistent with increased upwelling, which increases cool sea-breeze flows and its associated coastal stratus.

The consideration of T_{max} coastal cooling and inland warming areas in a single basin-wide dataset in past studies resulted in small trends, as the two effects almost cancel out. Such ''contaminated'' T_{max} values then also must contaminate the corresponding T_{ave} and DTR results (i.e., they also thus will not show significant trends). The lack of significant trends for the current all-California T_{max}, T_{ave}, and DTR results thus supports the current hypothesis.

As sea-breeze flows are driven by gradients of ocean-to-inland sea level pressure p_s, the spatial distribution of 1979–2002 p_s trend at 1000 LT was calculated from JJA average ECMWF ERA-40 high-resolution (i.e., Gaussian T85 grid, with a 1.4° grid resolution) model output. Results (Fig. 7) show pressure increases (up to 0.34 hPa decade^{-1}) in the overocean Pacific high and decreases in both the Nevada (up to −0.80 hPa decade^{-1}) and (smaller and more southerly) Death Valley (up to −0.68 hPa decade^{-1}) thermal lows. These changes could arise from an increased upward motion in the thermal lows resulting from the GHG-induced inland warming and thus from an increased induced downward motion in the Pacific high.

The corresponding temporal trend in the gradient of p_s was calculated separately for the SFBA and SoCAB areas from their overocean minus their overland p_s trends (i.e., grid points at ends of solid lines in Fig. 7). Results (Fig. 8) showed a larger trend at SoCAB than at SFBA (0.11 versus 0.04 hPa 100 km^{-1} decade^{-1}), both statistically significant with p values below 0.01. This result supports the current hypothesis of increased sea-breeze activity.

Nemani et al. (2001) attributed increased annual T_D values in coastal California to increased SST values (and their increased evaporation rates), and thus the 1950–75 and 1975–2005 average JJA daily averaged SST trends were plotted for the ocean area of Fig. 1. Results (Fig. 9) showed trends of 0.02° and 0.15°C decade^{-1}, respectively. A possible associated increase in coastal stratus could explain why, as noted above, coastal cooling T_{min} values (Fig. 6b) have increased faster than the corresponding inland warming values (Fig. 6a) (i.e., as a result of increased early evening trapping of coastal outgoing terrestrial radiation).

The increased rate of California coastal SST warming since 1976 (Fig. 9) has been associated with a concurrent PDO intensification (Ebbesmeyer et al. 1991), which has produced more frequent El Niño events (Trenberth and Hoar 1997; McGowan et al. 1998). Alfaro et al. (2006) and the current study (not shown) both showed warming summer all-California T_{ave} values strongly correlated with increased PDO index values, whereas LaDochy et al. (2007) and the current study (again not shown) both showed coastal T_{max} values uncorrelated with PDO. The explanation consistent with the current results is that the T_{max} values are contamination by the coastal cooling areas. It is, however, also possible that some of the current observed temperature trends could be associated with low-frequency decadal variability, expected even with a constant radiative forcing.

Goodridge (1991), Bereket et al. (2005), Duffy et al. (2007), and LaDochy et al. (2007) have attributed trends in T_{min} and/or T_{ave} to growing UHI effects. As Sacramento, Modesto, Stockton, and San José (Fig. 2a) have grown (DOT 2000) in aerial extent (21%–59%) and population (40%–118%), part of their observed increased JJA T_{max} values could be a result of increased daytime UHI intensity. Without UHI effects, the currently observed JJA SFBA coastal cooling area might have expanded to include these sites, as the first three are adjacent to rural airport sites that showed cooling T_{max} values resulting from increased marine influences. In addition, all urbanized sites with decreasing T_{max} values would probably show even larger cooling rates if UHI effects could be removed. The ''reverse'' asymmetric warming (i.e., T_{max} trend > T_{min} trend) and thus the increasing (and not the expected decreasing) DTR values at the inland warming sites noted above, however, might be because of growing daytime UHIs.

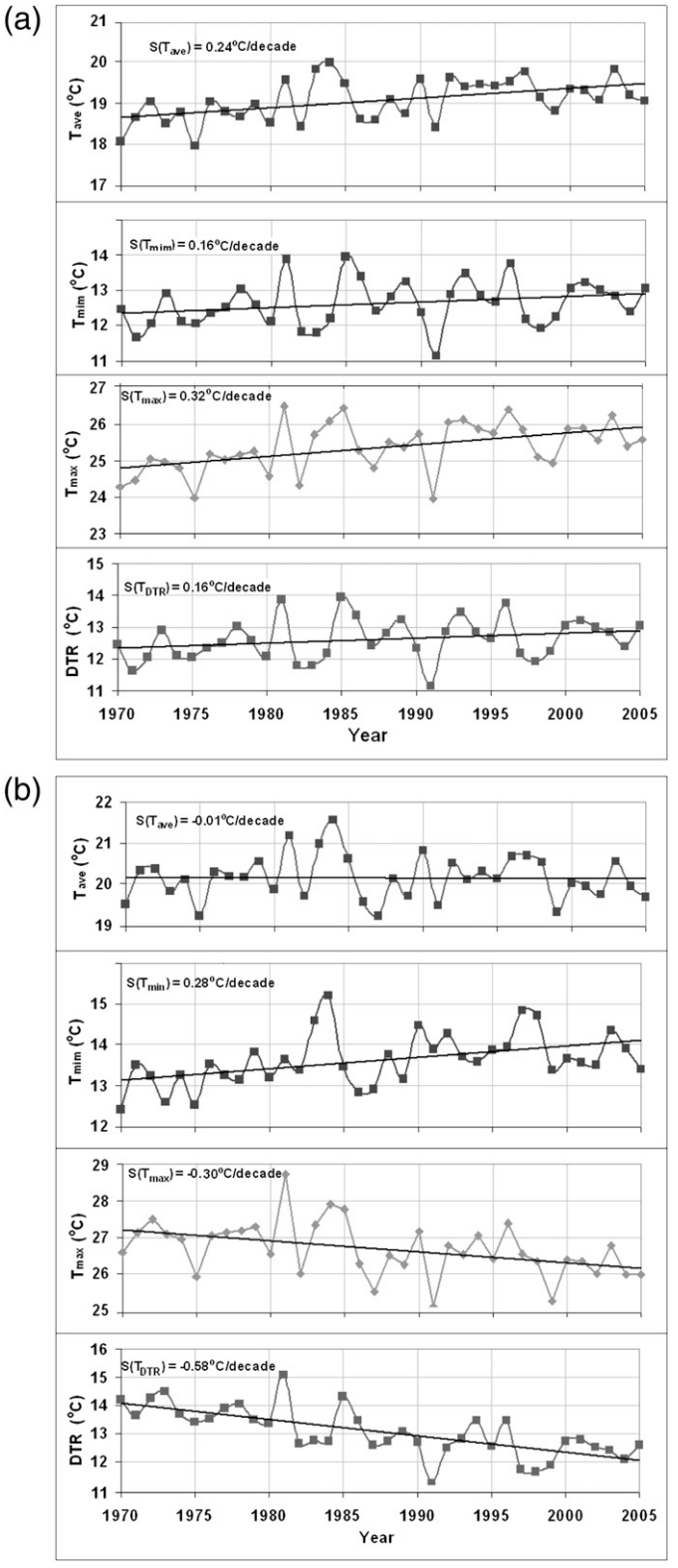

FIG. 6. Combined SFBA and SoCAB 1970–2005 summer 2-m temperature trends (°C decade^{-1}) of average, maximum, minimum, and range (DTR) values for (a) inland warming and (b) coastal cooling areas.

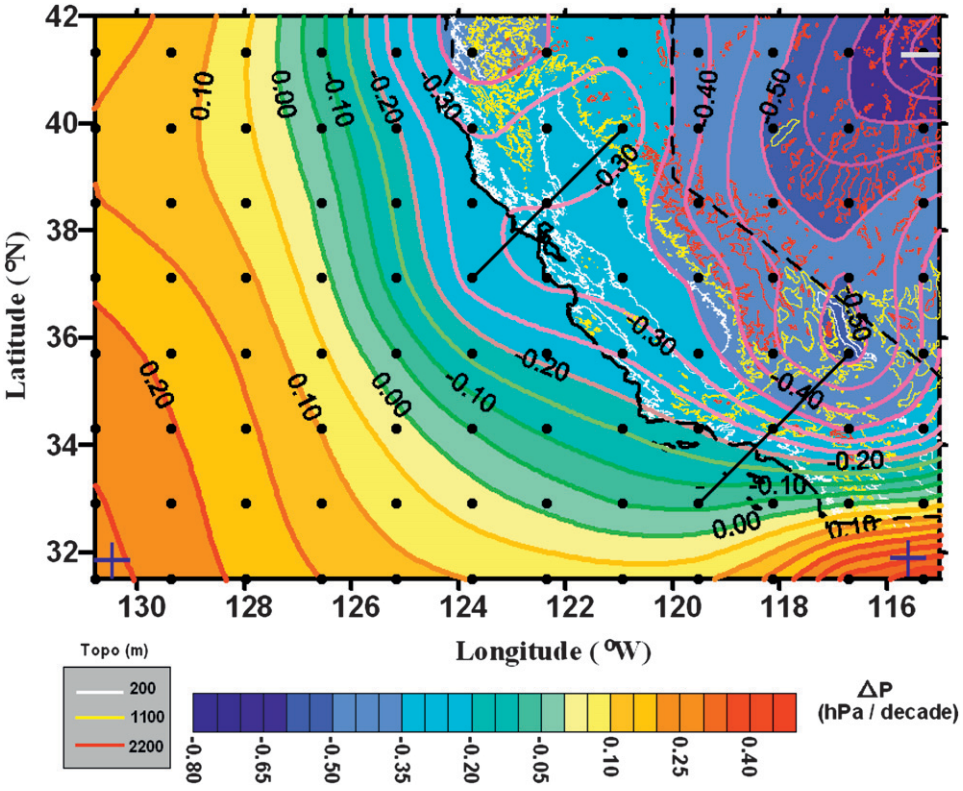

FIG. 7. Trend in 1979–2002 T85 ERA40 reanalysis of 1800 UTC summer sea level pressure changes (hPa decade^{-1}), where dots indicate 1.4° gridpoint locations and where endpoints of solid lines denote data points for pressure gradient trend calculation of Fig. 8; key topographic heights of 200, 1100, and 2200 m are shown by white, yellow, and red lines, respectively.

To determine if GCM models can discern the coastal cooling effects in the current results, 1950–99 JJA median (of 11 models) GCM 2-m T_{ave} values over California were determined. Results (Fig. 1) show warming rates that decrease from 0.13°C decade^{-1} at inland California to 0.08°C decade^{-1} at coastal areas north of the SoCAB. Although this ensemble result correctly shows coastal influences on T_{ave}, its coarse spatial resolution does not sufficiently resolve local topographic features and thus the finescale near-surface flow features that produced the coastal cooling of T_{max} values seen in current analysis of COOP data.

Of course, the possibility cannot be ruled out that the observed geographic differences in time trends during 1970–2005 could be a manifestation of low-frequency natural decadal-to-century-scale climatic variability. In principle, much longer time series in a stable climate regime would be needed to assess how often such geographically differentiated patterns of temperature time trends would arise by chance during such a 36-yr period. We are encouraged, however, that the observed geographic patterns of warming and cooling are geographically coherent and appear to be physically meaningful. Future research should seek to identify consistent correlates of warming and cooling at small geographic scales within the context of regional and global climate models.

5. Conclusions

The study evaluated 1950–2005 summer (JJA) mean monthly 2-m air temperatures from 253 California COOP sites, with a focus on the SoCAB and SFBA air basins and on the rapid post-1970 warming period. Daily COOP T_{min} and T_{max} values were used to produce average monthly values, and temporal trends were calculated for each site, all sites combined, and the combined SoCAB and SFBA regions. The goal was to elucidate a richer detail of observed temperatures than previously done. Spatial distributions of observed T_{max} trend values for each of the two air basins were thus constructed, with summertime climatological surface wind patterns overlaid to aid their interpretation.

Temporal trends in coastal sea level pressure gradient were also calculated from ECMWF ERA-40 reanalysis pressure values to estimate changes in sea-breeze activity

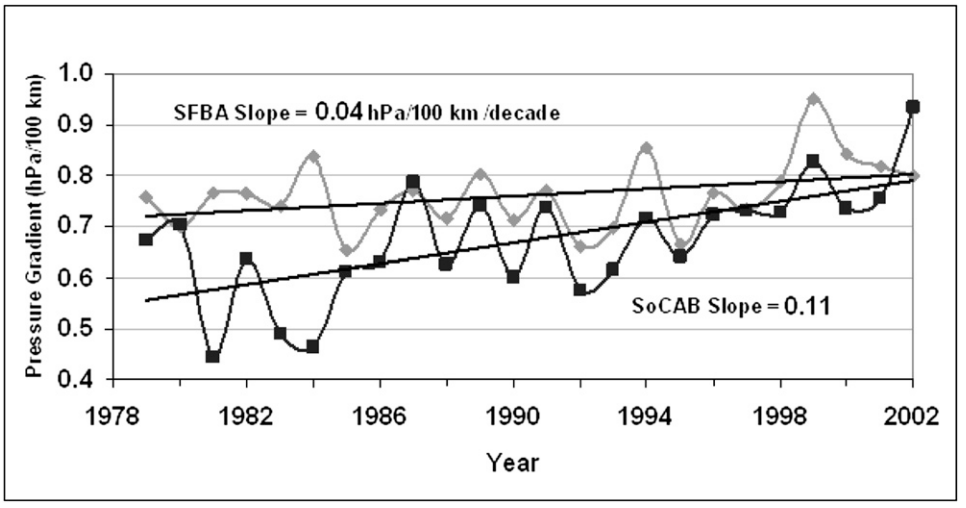

FIG. 8. Trends in ocean minus land summer 1800 UTC sea level pressure gradient (hPa 100 km^{-1} $decade^{-1}$) for SFBA (red) and SoCAB (blue) basins, calculated from values at grid points at ends of lines in Fig. 7.

in the SoCAB and SFBA. IPCC predicted 2-m JJA surface T_{ave} values were also interpolated to a 0.5° resolution grid over California.

The most significant result of the current study is that the expected GHG-driven global warming of summer T_{max} values in the eastern inland CenV and Sierra Nevada foothills may have produced enhanced cool-air sea-breeze intrusions and thus may have induced the currently observed cooling of summer T_{max} values in low-elevation coastal basins. This regional effect appears to coexist with the increases in California-wide daily T_{max}, T_{min}, and T_{ave} values and with increases in summer T_{min} values in both basins.

Results for all California COOP sites together showed increased JJA T_{ave} values; asymmetric warming, as T_{min} values increase faster than T_{max} values; and thus decreased DTR values. Spatial distributions of observed SoCAB and SFBA 1970–2004 JJA T_{max} values exhibited a complex pattern, with cooling in low-elevation coastal areas open to marine air penetration and warming at both inland and higher-elevation coastal areas. Although previous studies also found decreased JJA DTR values for these valleys, the current study showed that the decrease arose from small increases at the inland warming sites combined with large decreases at the coastal cooling sites.

Previous studies have suggested that the cooling of JJA T_{max} values in coastal California were a result of increased irrigation, coastal upwelling, or cloud cover, whereas the current hypothesis is that it arises from GHG-induced global warming of inland warming areas, which results in increased sea-breeze flow activity,

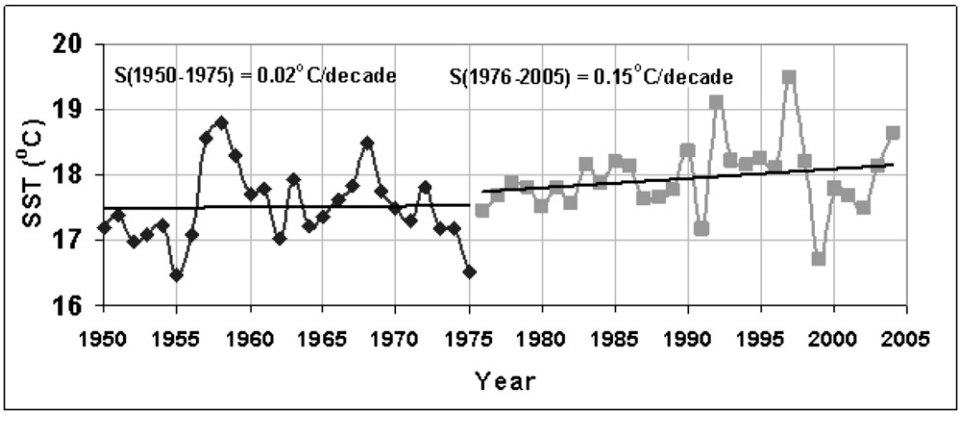

FIG. 9. Trend in summer average SSTs (°C $decade^{-1}$) for 1950–75 and 1975–2005 for ocean area of Fig. 1.

which in turn overwhelms warming in coastal cooling areas. This is consistent with the increased upwelling in the literature, which increases sea-breeze flows and thus coastal stratus. The spatial distribution of surface pressure changes showed pressure increases in the oceanic Pacific high and decreases in the inland California thermal low. Corresponding temporal increases in the SoCAB and SFBA coastal pressure gradients are supportive of the hypothesis of increased sea-breeze activity. It is, however, also possible that some of the current observed temperature trends could be associated with low-frequency decadal variability, expected even with a constant radiative forcing.

Previous studies have attributed increases in California JJA T_{min} and/or T_{ave} to UHI effects, which could also affect the currently observed T_{max} increases. As inland CenV cities have experienced growth in aerial extent and population, part of their currently observed increases in T_{max} could be due to increased daytime UHIs. Without this effect, the currently observed SFBA coastal cooling area might have been expanded to include these sites. All urbanized coastal sites with cooling T_{max} values probably would show even larger cooling trends if UHI effects could be removed.

GCM model T_{ave} values showed warming that decreases from inland California to coastal areas. Although this correctly shows coastal influences on T_{ave}, its coarse spatial resolution does not allow it to sufficiently resolve the local topographic and thus finescale near-surface flow features that produced the coastal cooling of T_{max} values in current analysis. California coastal cooling of annual T_{ave} values, however, is seen as a single data point in the global 2001 IPCC observational dataset.

Additional observational studies and/or downscaled model results (to mesoscale models with 1–10-km grid resolution) are thus necessary to determine the finescale structure and the more precise boundaries between the adjacent inland warming and coastal cooling areas found in the current results. In addition, additional SST, sea-breeze (e.g., onshore wind speed and cloud cover), agricultural irrigation, and UHI effects need further analysis and model simulations. These analyses and simulations might be able to determine if the sea-breeze flows start earlier, are more common, are colder, and/or last longer.

The observed coastal cooling may thus be an example of a regional reverse reaction to GHG warming, and significant societal impacts in California may result from this effect. For example, agricultural production could increase or decrease (e.g., wine grape production will increase in the cooling valleys north of San Francisco). Beneficial effects due to reduced summer T_{max} values in coastal areas could include decreased maximum O_3 levels, which will occur as a result of reduced fossil fuel usage for cooling, reduced natural hydrocarbon production, and reduced photochemical photolysis rates. Human thermal-stress rates and mortality will also decrease. Additional analyses and simulations are needed to evaluate T_{max} cumulative frequency distributions to see if heat wave frequency is increasing at a given site, even as average T_{max} values decrease.

Although similar GHG-induced reverse reactions could be expected in other subtropical low-elevation coastal regions, other similar impacts might also exist in areas of high topography, as with the cooling found along the California–Nevada border. Such possibilities require further investigation by additional regional-scale data analyses and/or dynamically downscaled numerical modeling.

Acknowledgments. The authors thank Prof. Alan Robock of Rutgers University for his insightful comments. We also thank the School of Engineering, Santa Clara University for funding the lead author. We also acknowledge the Program for Climate Model Diagnosis and Intercomparison (PCMDI) for collecting and archiving CMIP3 model output and the WCRP Working Group on Coupled Modelling (WGCM) for organizing the model data analysis. The WCRP CMIP3 multimodel dataset is supported by the Office of Science, U.S. Department of Energy.

REFERENCES

Abatzoglou, J. T., K. T. Redmond, and L. E. Edwards, 2009: Classification of regional climate variability in the state of California. *J. Appl. Meteor. Climatol.,* in press.

Alfaro, E. J., A. Gershunov, and D. Cayan, 2006: Prediction of summer maximum and minimum temperature over the central and western United States: The role of soil moisture and sea surface temperature. *J. Climate,* **19,** 1407–1421.

Bakun, A., 1990: Global climate change and intensification of coastal ocean upwelling. *Science,* **247,** 198–201.

Bereket, L., D. Fabris, J. E. Gonzalez, S. Chiappari, N. L. Miller, and R. Bornstein, 2005: Climatology temperature mapping for California urban heat islands. *Bull. Amer. Meteor. Soc.,* **86,** 1542–1543.

Betts, R. A., 2001: Biogeophysical impacts of land use on present-day climate: Near-surface temperature change and radiative forcing. *Atmos. Sci. Lett,* **2,** 39–51.

Blumenthal, D., T. Smith, D. Lehrman, R. A. Rasmussen, G. Z. Whitten, and R. A. Bazter, 1985: Southern San Joaquin Valley ozone study. California Air Resource Board Final Rep. ST199092-981-D, 143 pp.

Bonfils, C., and P. B. Duffy, 2007: Comments on ''Methodology and results of calculating central California surface temperature trends: Evidence of human-induced climate change?'' *J. Climate,* **20,** 4486–4489.

——, and D. Lobell, 2007: Empirical evidence for a recent slowdown in irrigation-induced cooling. *Proc. Natl. Acad. Sci. USA,* **104,** 13 582–13 587, doi:10.1073/pnas.0700144104.

Bornstein, R. D., 1968: Observations of the urban heat island effect in New York City. *J. Appl. Meteor.,* **7,** 575–582.

Boucouvala, D., R. Bornstein, J. Wilkinson, and D. Miller, 2003: MM5 simulations of a SCOS97-NARSTO episode. *Atmos. Environ.,* **37** (Suppl.), 95–117.

CARB, 1989: Proposed identification of districts affected by transported air pollutants. California Air Resources Board Research Rep., 92 pp.

Chase, T., R. Pielke Sr., T. Kittel, R. Nemani, and S. Running, 2000: Simulated impacts of historical land cover changes on global climate in northern winter. *Climate Dyn.,* **16,** 93–105.

Christy, J. R., W. B. Norris, K. Redmond, and K. P. Gallo, 2006: Methodology and results of calculating central California surface temperature trends: Evidence of human-induced climate chage? *J. Climate,* **19,** 548–563.

Defries, R. S., L. Bounoua, and G. J. Collatz, 2002: Human modification of the landscape and surface climate in the next fifty years. *Global Change Biol.,* **8,** 438–458.

DOT, 2000: Highway statistics 2000. U.S. Department of Transportation Federal Highway Administration. [Available online at http://www.fhwa.dot.gov/ohim/hs00/hm72.htm.]

Duffy, P. B., C. Bonfils, and D. Lobell, 2007: Interpreting recent temperature trends in California. *Eos, Trans. Amer. Geophys. Union,* **88,** 409, doi:10.1029/2007EO410001.

Ebbesmeyer, C., D. Cayan, D. McLain, F. Nichols, D. Peterson, and K. Redmond, 1991: 1976 step in the Pacific climate: Forty environmental changes between 1968–1975 and 1977–1984. *Proceedings of the Seventh Annual Pacific Climate (PACLIM) Workshop, Interagency Ecological Program,* Tech. Rep. 26, J. Betancourt and V. Tharp, Eds., California Dept. Water Resources, 115–126.

Gallo, K. P., A. L. McNab, T. R. Karl, J. F. Brown, J. J. Hood, and J. D. Tarpley, 1993: The use of a vegetation index for assessment of the urban heat island effect. *Int. J. Remote Sens.,* **14,** 2223–2230.

Gilliland, R. P., 1980: The structure and development of the California heat trough. M.S. thesis, Dept. of Meteorology, San Jose State University, 90 pp.

Giorgis, R. B., 1983: Meteorological influence on oxidant distribution and transport in the Sacramento Valley. Ph.D. thesis, University of California, Davis, 124 pp.

Goodridge, J. D., 1991: Urban bias influence on long-term California air temperature trends. *Atmos. Environ.,* **26B,** 1–7.

Hayes, T. P., J. J. R. Kinney, and N. J. M. Wheeler, 1984: California surface wind climatology. California Air Resources Board, Research Rep., 79 pp. [Available from California Air Resources Board, Aerometric Data Division, 2020 L St., Sacramento, CA 95814.]

Herbert, T. D., and J. D. Schuffert, 2001: Collapse of the California current during glacial maxima linked to climate change on land. *Science,* **293,** 71–76.

Hickey, B. M., 1979: The California current system—Hypotheses and facts. *Prog. Oceanogr.,* **8,** 191–279.

Jin, M., 2004: Analyzing skin temperature variations from long-term AVHRR. *Bull. Amer. Meteor. Soc.,* **85,** 587–600.

Karl, T. R., and Coauthors, 1993: A new perspective on recent global warming: Asymmetric trends of daily maximum and minimum temperature. *Bull. Amer. Meteor. Soc.,* **74,** 1007–1023.

Kueppers, L. M., M. A. Snyder, and L. C. Sloan, 2007: Irrigation cooling effect: Regional climate forcing by land-use change. *Geophys. Res. Lett.,* **34,** L03703, doi:10.1029/2006GL028679.

LaDochy, S., R. Medina, and W. Patzert, 2007: Recent California climate variability: Spatial and temporal patterns in temperature trends. *Climate Res.,* **33,** 159–169.

Landsberg, H. E., 1981: *The Urban Climate.* Academic Press, 275 pp.

Lawton, R. O., U. S. Nair, R. A. Pielke Sr., and R. M. Welch, 2001: Climatic impact of tropical lowland deforestation on nearby montane cloud forests. *Science,* **294,** 584–587.

Lobell, D., and C. Bonfils, 2008: The effect of irrigation on regional temperatures: A spatial and temporal analysis of trends in California, 1934–2002. *J. Climate,* **21,** 2063–2071.

——, G. Bala, C. Bonfils, and P. B. Duffy, 2006: Potential bias of model projected greenhouse warming in irrigated regions. *Geophys. Res. Lett.,* **33,** L13709, doi:10.1029/2006GL026770.

MacKay, K., 1997: Ozone over San Francisco: Means and patterns during pollution episodes. Dept. of Meteorology, San Jose State University Research Rep. EPA-600/4-77-046, 55 pp.

Mann, P. S., 2007: *Introductory Statistics*. 6th ed. J. Wiley, 615 pp.

Maurer, E. P., 2007: Uncertainty in hydrologic impacts of climate change in the Sierra Nevada, California, under two emissions scenarios. *Climatic Change,* **82,** 309–325.

McElroy, J. L., and T. B. Smith, 1991: Lidar descriptions of mixing-layer thickness characteristics in a complex terrain/coastal environment. *J. Appl. Meteor.,* **30,** 585–597.

McGowan, J. A., D. R. Cayan, and L. M. Dorman, 1998: Climate-ocean variability and ecosystem response in the northeast Pacific. *Science,* **281,** 210–217.

McGregor, H. V., M. Dima, H. W. Fischer, and S. Mulitzal, 2007: Rapid 20th-century increase in coastal upwelling off northwest Africa. *Science,* **315,** 637–639.

Miller, N. L., and N. J. Schlegel, 2006: Climate change projected fire weather sensitivity: California Santa Ana wind occurrence. *Geophys. Res. Lett.,* **33,** L15711, doi:10.1029/2006GL025808.

Mintz, Y., 1984: The sensitivity of numerically simulated climates to land-surface boundary conditions. *The Global Climate,* J. Houghton, Ed., Cambridge University Press, 79–105.

Nair, U. S., R. O. Lawton, R. M. Welch, and R. A. Pielke Sr., 2003: Impact of land use on Costa Rican tropical montane cloud forests: Sensitivity of cumulus cloud field characteristics to lowland deforestation. *J. Geophys. Res.,* **108,** 4206, doi:10.1029/2001JD001135.

Nemani, R. R., M. A. White, D. R. Cayan, G. V. Jones, S. W. Running, and J. C. Coughlan, 2001: Asymmetric warming over coastal California and its impact on the premium wine industry. *Climate Res.,* **19,** 25–34.

Pielke, R. A., Sr., G. Marland, R. A. Betts, T. N. Chase, J. L. Eastman, J. O. Niles, D. D. Niyogi, and S. W. Running, 2002: The influence of land-use change and landscape dynamics on the climate system: Relevance to climate-change policy beyond the radiative effect of greenhouse gases. *Philos. Trans. Roy. Soc. London,* **360A,** 1705–1719.

——, and Coauthors, 2007: Unresolved issues with the assessment of multidecadal global land surface temperature trends. *J. Geophys. Res.,* **112,** D24S08, doi:10.1029/2006JD008229.

Pon, B., D. M. Stamper-Kurn, C. K. Smith, and H. Akbari, 2000: Existing climate data sources and their use in heat island research. LBNL Tech. Rep. LBL41973, 20 pp.

Root, H. E., 1960: San Francisco, the air conditioned city. *Weatherwise,* **13,** 47–54.

Seaman, N. L., D. R. Stauffer, and A. M. Lario-Gibbs, 1995: A multiscale four-dimensional data assimilation system applied in the San Joaquin Valley during SARMAP. Part I: Modeling design and basic performance characteristics. *J. Appl. Meteor.,* **34,** 1739–1761.

Simpson, J. J., 1983: Large-scale thermal anomalies in the California current during the 1982-1983 El Niño. *Geophys. Res. Lett.,* **10,** 917–940.

Smith, T. M., and R. W. Reynolds, 2003: Extended reconstruction of global sea surface temperature based on COADS data (1954–1997). *J. Climate,* **16,** 1495–1510.

Snyder, M. A., L. C. Sloan, N. S. Differbaugh, and J. L. Bell, 2003: Future climate change and upwelling in the California current. *Geophys. Res. Lett.,* **30,** 1823, doi:10.1029/2003GL017647.

Stenchikov, G. L., and A. Robock, 1995: Diurnal asymmetry of climatic response to increased CO_2 and aerosols: Forcings and feedbacks. *J. Geophys. Res.,* **100,** 26 211–26 227.

Trenberth, K., and T. Hoar, 1997: El Niño and climate change. *Geophys. Res. Lett.,* **24,** 3057–3060.

Walters, J. T., R. T. McNider, X. Shi, W. B. Norris, and J. R. Christy, 2007: Positive surface temperature feedback in the stable nocturnal boundary layer. *Geophys. Res. Lett.,* **34,** L12709, doi:10.1029/2007GL029505.

Williams, W., and R. DeMandel, 1966: Land-sea boundary effects on small scale circulations. Meteorology Dept., San Jose State University Progress Rep. 2, 97 pp.

Zhang, H., A. Henderson-Sellers, and K. McGuffie, 1996: Impacts of tropical deforestation. Part II: The role of large-scale dynamics. *J. Climate,* **10,** 2498–2522.